Precision Engineering 59 (2019) 134–149

Contents lists available at ScienceDirect

Precision Engineering

journal homepage: www.elsevier.com/locate/precision

Thermal effects compensation and associated uncertainty for large magnet assembly precision alignment

I. Doytchinov[a,b,*], P. Shore[b,c], B. Nicquevert[a], X. Tonnellier[b], A. Heather[b], M. Modena[a]

[a] European Council for Nuclear Research - CERN, Route de Meyrin 385, 1217 Meyrin, Switzerland
[b] Cranfield University Precision Engineering Institute, College Rd, Cranfield, MK43 0AL, United Kingdom
[c] National Physical Laboratory - NPL (United Kingdom), Hampton Road, Teddington, TW11 0LW, United Kingdom

ARTICLE INFO

Keywords:
Accelerator magnets
Precision alignment
Thermal error compensation
Digital twins
FEM modelling
Uncertainty modelling
Empirical modelling
Metamodeling

ABSTRACT

Big science and ambitious industrial projects continually push technical requirements forward beyond the grasp of conventional engineering techniques. An example of these are the extremely tight micrometric assembly and alignment tolerances required in the field of celestial telescopes, particle accelerators, and the aerospace industry. Achieving such extreme requirements for large assemblies is limited, largely by the capability of the metrology used, namely, its uncertainty in relation to the alignment tolerance required. The current work described here was done as part of Maria Curie European research project held at CERN, Geneva. This related to future accelerators requiring the spatial alignment of several thousand, metre-plus large assemblies to a common datum within a targeted combined standard uncertainty ($u_c^{tg}(y)$) of 12 µm. The current work has found several gaps in knowledge limiting such a capability. Among these was the lack of uncertainty statements for the thermal error compensation applied to correct for the assembly's dimensional instability, post metrology and during assembly and alignment. A novel methodology was developed by which a mixture of probabilistic modelling and high precision traceable reference measurements were used to quantify the uncertainty of the various thermal expansion models used namely: Empirical, Finite Element Method (FEM) models and FEM metamodels. Results have shown that the suggested methodology can accurately predict the uncertainty of the thermal deformation predictions made and thus compensations. The analysis of the results further showed how using this method a 'digital twin' of the engineering structure can be calibrated with known uncertainty of the thermal deformation behaviour predictions in the micrometric range. Namely, the Empirical, FEM and FEM metamodels combined standard uncertainties ($u_c(y)$) of prediction were validated to be of maximum: 8.7 µm, 11.28 µm and 12.24 µm for the studied magnet assemblies.

1. Introduction

Large-scale scientific and industrial research projects require state of the art engineering to fulfil the desired requirements. In such projects, micrometre accuracy of assembly and alignment of large components can be critical. Alignment of large structures is defined as the procedure where large components or assemblies are dimensionally arranged into a superstructure to deliver certain desired functions at a given tolerance. This process can be performed actively by the use of actuators and guidance systems [1] or passively by reliance on well-designed kinematic features and tight manufacturing tolerances [2]. "Large" can be defined as any component or assembly that is challenging to measure to a low uncertainty by industrial high-performance Coordinate Measurement Machines (CMMs) or as defined by Ref. [3] larger than 1 m. In the alignment of subassemblies into a superstructure, one needs to know the location of the subassembly feature of interest with respect to its' global reference for alignment. For the alignment of particle accelerators, the feature of importance is the magnetic axis, or as defined in Refs. [4,5] location within each focusing magnet aperture at which the magnetic field is minimum or null. The global reference for alignment is most commonly a network of stable stretched wires or lasers [5–7]. In particle accelerators, magnets are used as electromagnetic lenses, directing and focusing the accelerated particles to the desired experimental stage. Small misalignments of the focusing magnets electromagnetic axis can lead to significant errors over the large machine size and cause downgraded collisions and detection rates in the experiment detectors [8] (Fig. 1).

The motivation of this work comes from the tight requirements concerning the alignment of components in the Compact Linear Collider study (CLIC) [9] for the future 40 km range linear accelerator.

* Corresponding author. European Council for Nuclear Research - CERN, Route de Meyrin 385, 1217 Meyrin, Switzerland.
E-mail addresses: Jordan.Doitchinov@gmail.com, Iordan.doytchinov@epfl.ch (I. Doytchinov).

https://doi.org/10.1016/j.precisioneng.2019.06.005
Received 28 November 2018; Received in revised form 5 June 2019; Accepted 9 June 2019
Available online 12 June 2019
0141-6359/

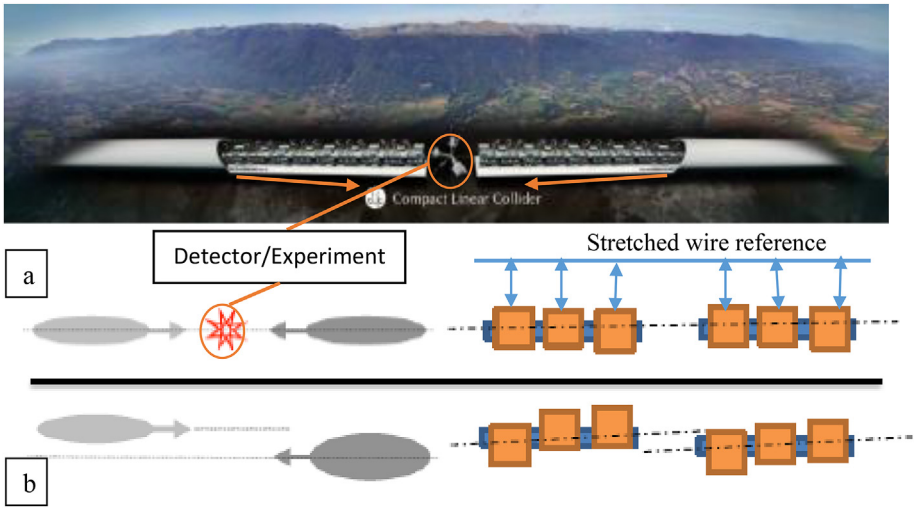

Fig. 1. Top: CLIC 40 km + concept impression, Jura mountains, Genevois. Bottom: a) Beam bunches collide due to successful alignment of accelerator active components. b) Beam bunches missing collision due to unsuccessful alignment of accelerator components.

The alignment tolerance of each magnetic axis of CLIC components should be within a 12 μm (1 σ) cylindrical uncertainty zone with respect to a global reference. The global reference is provided by a series of overlapping stretched wires, each one of 200 m length [7] (Fig. 1).

To achieve global alignment of all active magnetic components, a multiple step procedure of pre-alignment measurements and active positioning with the help of ultra-precision actuators is envisaged [7,10]. In this procedure, the ultra-precision actuators are to be used for positioning the subassemblies and their magnetic axis to their desired aligned location with respect to a stretched wire used as a global reference as shown in (Fig. 2).

In this figure a heavily simplified sketch of the smallest CLIC 'T1' series assembly as shown further in (Fig. 3). The largest magnet assembly model 'T4' has identical geometry as T1 but with length near to 2 m instead of the 629 mm shown in (Fig. 3).

In advance of the active alignment procedure, calibration (pre-alignment) measurements would be required as input information for the actuation system. Pre-alignment measurements quantify the spatial location of each focusing magnet's electromagnetic axis (Fig. 2 (A)) with respect to each assembly's local coordinate frame. The spatial location of each magnet electromagnetic axis is defined/realized by best fitting a thin stretched wire to its location via a magnetic measurement system [4,11]. Following the magnet axis defining thin wire is measured with respect to the local for each assembly coordinate frame defined by multiple (more than three) spherical measurement targets called fiducials (Fig. 2 (B)). All those procedures are done in the same place and time - by high-performance multisensory CMM system using a mixture of non-contact and tactile measurement probes. The sphere fiducials defining each assembly coordinate frame (Fig. 2 (B)) are rigidly fixed to each assembly and linked by a kinematic coupling to the removable Wire Positioning System (WPS). The WPS is a high precision non-contact sensor [12,13] measuring the absolute spatial location of fiducials/assembly with respect to the global tunnel reference – a stretched wire (different than the one used of the magnet axis measurement). The sensors provide absolute 2 D coordinates of a stretched wire canter with respect to its own mounting base. It operates on capacitive-based principle and was developed and calibrated bespoke for wire-based alignment in accelerators. It has an evaluated standard measurement uncertainty of below 1 μm [13,14]. In this way, the complete metrology frame is measured/closed and the spatial location of each magnet axis is known with respect to the global alignment reference – the tunnel stretched wire. Following the pre-alignment

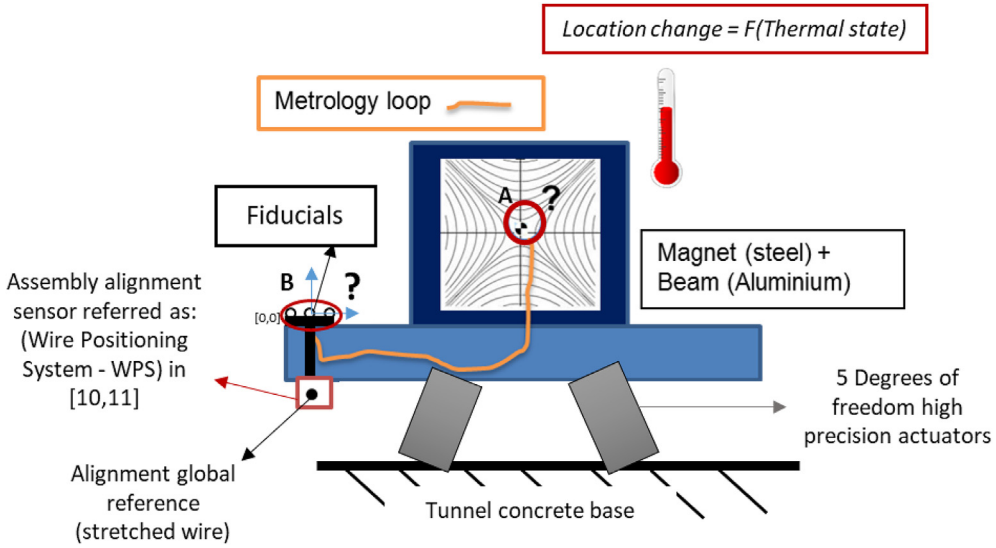

Fig. 2. Simplified cross-section sketch of magnet assembly with a quadrupole focusing magnet axis - A and assembly local coordinate frame defined by network of spherical fiducials – B.

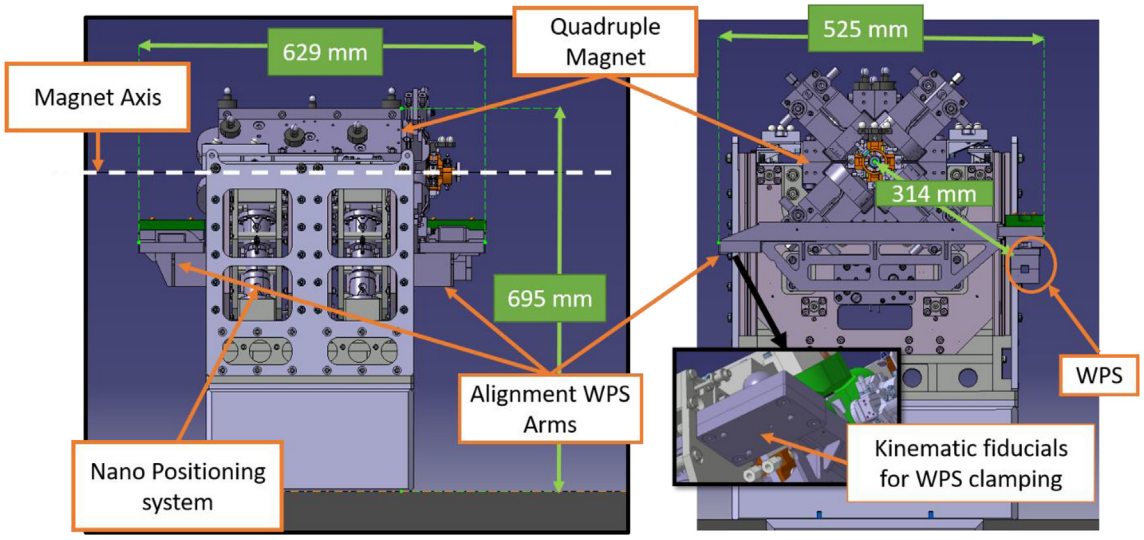

Fig. 3. CLIC T1 Module prototype CAD, Left: Side view, Right: Front view.

procedures performed in a metrology laboratory, assemblies are envisaged to be transported and installed in the accelerator tunnel. Once installed they will be actively aligned and stabilized during accelerator machine operation with the help of 5° of freedom ultra-precision actuators [9] (Figs. 2 and 3).

The largest and most critical contributor to the alignment uncertainty budget is linked to the pre-alignment measurements. The spatial location of each magnetic axis (A Fig. 2) with respect to the local coordinate frame of each assembly (B Fig. 2) has to be known during accelerator operation to a targeted standard uncertainty ($u_c^{tg}(y)$) of 12 µm (Fig. 4). The required combined magnetic, non-contact and tactile measurements are at the limit of today's' three-dimensional metrology performances for 2 m size assemblies. Moreover, temperatures of the assemblies during alignment and operation can vary significantly from that experienced during metrology. This temperature variation can cause large thermal deformations that need to be compensated, and the uncertainty of the compensation accounted for in the alignment budget. The measurement performance required for this procedure and the required knowledge of the geometrical state of the assemblies during accelerator machine operation makes this task extremely challenging.

In Particle Accelerator Components' Metrology and Alignment to the Nanometre-scale (PACMAN) program [6] held at CERN, strategies were studied on how this targeted uncertainty could be realistically achieved. This included the evaluation of the task-specific uncertainty for the metrology procedures performed in a controlled laboratory environment and simulating and measuring the expected thermal effects during accelerator operation conditions. For this purpose we developed and integrated magnetic, electric axis metrology and geometrical survey in one place and time - the measurement environment of a high accuracy CMMs (Coordinate Measurement Machine) (Fig. 5, a)).

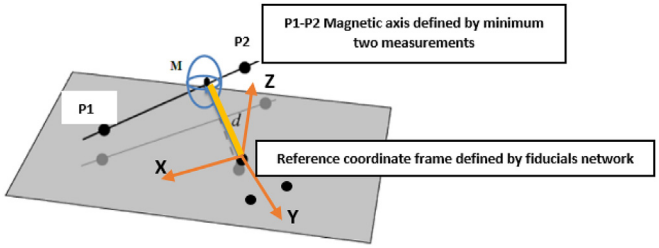

Fig. 4. The pre-alignment metrology defined as: spatial location (with uncertainty) of the magnetic axis (defined by minimum two 3D coordinates P1-P2) with respect to each assembly local coordinate frame (defined by minimum 3 fiducial spheres at the centre of one them).

The pre-alignment measurements were performed with temperature stability of ± 0.1 °C (ISO 14644-1 Class 1 metrology thermal environment) with a magnet powered at the minimum current required for magnetic axis measurement (4 A was chosen as detailed in Ref. [11] as the minimum amperage required for axis measurement). This low current level was employed to verify the optimum performance of our metrology system under stable temperature conditions with minimal thermal effects (and consequently dimensional instabilities). Magnetic water cooling was not employed during measurement in order to minimize potential vibrations or thermal loads induced by the fluid flow. The full task-specific uncertainty evaluation for this pre-alignment experiment (including any biases due to amperage current heating) was estimated to be in the order of 7 µm (1s) and complete method and procedure communicated in Ref. [15]. Although pre-alignment measurements were within the desired budget at the tightly controlled thermal conditions in the laboratory [15], these would not hold during the alignment procedure inside the accelerator tunnel under operational conditions. Alignment (and thus metrology data) would be needed when the measurand/assembly is fully operational and subject to; a high coil current, water cooling in operation and influence from surrounding tunnel air streams. This change in thermal conditions would create an expected internal thermal field gradient of 10 °C or more for the assembly components temperature compared to that experienced during metrology.

The change of the assembly's thermal profile during accelerator operation would create a shift of the magnetic axis with respect to the sphere fiducials spatial location, as initially measured at pre-alignment. This change can be defined as the *Total Thermal Deformation (TTD)* of assembly metrology frame. Any such TTD of the metrology frame should be quantified, corrected and the uncertainty of this correction U_{TTD} added to the bench measurements uncertainty $U_{Bench\ measurments}$ [µm] budget Eq. (1).

$$\overrightarrow{Pre-Alignment} = \left[\overrightarrow{Bench\ measurments} + \overrightarrow{TTD}\right] \pm U\ pre - alignment \quad (1)$$

where

$$U\ pre - alignment = \sqrt{U^2_{Bench\ measurments} + {U_{TTD}}^2}$$

In the PACMAN project, the uncertainty of alignment measurements within the laboratory ($U_{Bench\ measurments}$) were evaluated to be in the order

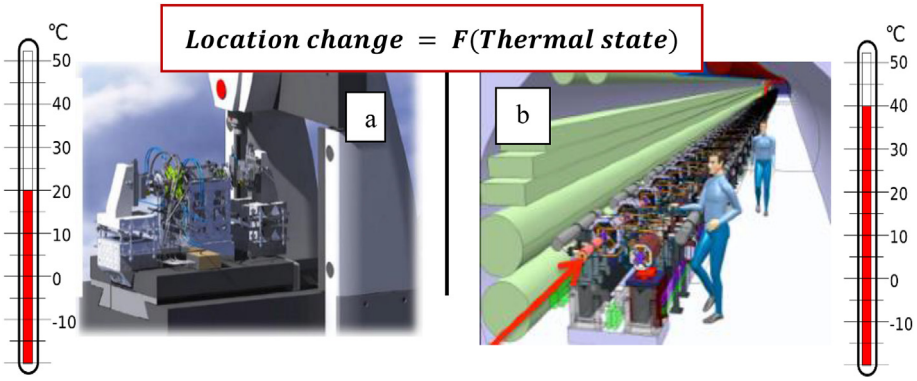

Fig. 5. a) Pre-alignment metrology completed in laboratory environment, b) Active alignment of components in tunnel i.e. operational environment.

of 6.91 μm–7.96 μm (1*s*) (depending on the size of assembly measured and CMM system used) [15]. This represented over 50% of the available 12 μm $u_c^{tg}(y)$ budget, leaving between 8.9 μm and 9.8 μm (1*s*) budget for the uncertainty (U_{TTD}) of applying a compensation for the TTD [15].

The total thermal drift could not be measured directly by the PACMAN integrated metrology system at the time of the campaign. The reason was that the bespoke non-contact wire axis measurement CMM head was in development and not available during the campaign. Thus the thermal drift was defined as the sum of the magnet axis and fiducial drifts to a common frame of reference to which both could be measured via alternative systems as detailed in Ref. [14]. The post metrology shift of the assembly fiducials and magnetic axis can be determined independently with respect to a common stable frame of reference, this being the magnet to 5 dof actuators mount base. In the current studies, this is referred/translated as the granite CMM table on which the simplified assembly is mounted via metrological cube as shown in Fig. 8. Thus, the TTD will be equal to the sum of the spatial shift of the fiducials [Total Fiducial Thermal Error (TFTE)] and spatial shift of the magnetic axis [Total Magnetic Axis Thermal Error (TMATE)] (2) with respect to the common reference fixed on the granite base. This being a coordinate system defined by four 1 cm (diameter) metrology spheres rigidly embedded on the granite base.

$$\overrightarrow{TTD} = \overrightarrow{TFTE} + \overrightarrow{TMATE} \tag{2}$$

where

$$\overrightarrow{TFTE} = (\overrightarrow{NDE_{fiducials}} \pm UNDE_{fiducials}) \tag{3}$$

and

$$\overrightarrow{TMATE} = (\overrightarrow{NDE_{magnetic\ axis}} \pm UNDE_{magnetic\ axis}) \tag{4}$$

where NDE = nominal differential expansion and UNDE = uncertainty of NDE.

$$\overrightarrow{TTD} = [\overrightarrow{NDE_{fiduciasls}} + \overrightarrow{NDE_{magnetic\ axis}} \pm U_{TTD} \text{where } U_{TTD} = f(UNDE_{fiducials}, UNDE_{magnetic\ axis}) \tag{5}$$

The U_{TTD} can be determined by either the analytical law of propagation of uncertainties or by Monte Carlo method (GUM Supplement 1 [16]) applied to the vector equation describing TTD in the local frame of reference. The TTD has to be measured or predicted and compensated for in each of the 20 000 envisaged magnet assemblies in the CLIC machine, with targeted uncertainty of $U_{TTD}^{tg} \leq 8.9$ μm (1s). This targeted prediction uncertainty with a traceability to the SI realisation of the unit of metre [17]. By traceable it means with an established and documented unbroken chain of calibrations with respect to SI unit definition, which all contribute to the measurement or prediction uncertainty [18]. Validating the feasibility of such an endeavour would fill one of the major technological gaps in the CLIC study. Direct online alignment measurements of magnet axis and fiducials during accelerator machine operation might not be an economically viable solution for 20 000 assemblies. Simulations and mathematical modelling, as studied in the state-of-art (summarised in Ref. [14]), do not provide valid statements of uncertainty, thus preventing their direct application to this scenario. These challenges acted as the main motivation for the authors.

In the current work, we proposed a method by which a valid statement of uncertainty (U_{TTD}) for applying a mathematical compensation model for the TTD can be evaluated. This was done by quantifying and distinguishing between bias [ε] and the variability [$V(x)^{1/2}$] of the mathematical models used for the deformation prediction. We performed and validated the method by proving we can successfully evaluate the uncertainty of three different types of thermal deformation prediction models used in CLIC context for the TTD prediction: an empirical, FEM and FEM meta-models (also known as surrogate FEM models). Our experience in validating this method for uncertainty estimation of thermal deformation model predictions can be considered significant and transferable to areas in precision engineering where the knowledge of modelling and prediction uncertainty can be critical.

2. Thermal effects modelling and associated uncertainty

Dimensions are inherently linked to the temperature at which they are measured. Measurements of an assemblies dimension taken at different thermal conditions have an error proportional to the expansion or contraction of the materials used for the assembly components and the nature of the assembly fixture and mechanical constraint [19–21]. The dimensional deformation of the alignment targets of interest can be defined as Nominal Differential Expansion (*NDE*). The uncertainty of the knowledge of *NDE* or any compensation applied for its correction in alignment metrology can be defined as U_{NDE}. Nominal expansion of solids and assemblies can be generalised in the following steps as discussed in Refs. [14,22–25] (Fig. 6).

The change in heat transfer conditions through an assembly body, or between the assembly the environment (including internal heat sources) can cause changes in the thermal field of the measurand. The change in the thermal field state is related to internal material stresses that cause dimensional deformation among the body or bodies of the measurand assembly. Any change of the heat transfer state acting on an assembly will create changes in the thermal field within its components thus causing them (and ultimately the assembly) to vary from its nominal dimensions, as defined during metrology. The thermal and dimensional changes from nominal conditions can be classified in three general ways: *Uniform temperature changes other than that during*

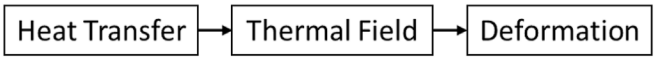

Fig. 6. Relationship between heat transfer and deformation.

metrology; *static temperature gradients deviating from metrology environment temperatures* and *dynamic thermal variation/gradients* [19]. In this work, a concentration on *static temperature gradients deviating from metrology environment temperatures* is made as most likely in the CLIC project context.

Change in thermal conditions via heat transfer (Convection, Conduction, Radiation) during machine operation after metrology would cause a change in the heat transfer state ΔQ_{state} and thus a change in the thermal field ($\overrightarrow{\Delta T_{field}}$) of the assembly components Eq. (6):

$$\overrightarrow{\Delta T_{field}} = f(\Delta Q_{state}) = f(\Delta Conduction,\ \Delta Convection,\ \Delta Radiation) \quad (6)$$

Change in the thermal field would cause internal strain and thus expansion in the various components of the assembly constrained in a way dictated by the mechanical assembly design and constraints. The combined effect of all assembly components nominal expansions (NE_i) (as guided by the assembly mechanical constraints) would define the final shift of the metrology frame. The metrology frame deformation can be defined as the deformation of an alignment feature (fiducial, or magnetic axis) B with respect to the magnet axis A. In the case of magnets, A can be the magnetic axis (Fig. 2 (A)) and B can represents an alignment fiducial mounted on the assembly (Fig. 2 (B)). Any shift of the location of A with respect to B would be due to the combined function of all dimensional deformations attributed to the assembly components defined as $\overrightarrow{NDE_{A-B}}$ – (*Nominal Differential Expansion of A with respect to B*) Eq. (7):

$$\overrightarrow{NDE_{A-B}} = \sum_{i=1}^{n} f\left(\overrightarrow{NDE_i}\right) = \sum_{i=1}^{n} f\left(\frac{\overrightarrow{\Delta L_i}}{\overrightarrow{L_i}}\right) = \sum_{i=1}^{n} f\left(\overline{\alpha_{L_i}} * \overrightarrow{\Delta T_{field_i}}\right) \quad (7)$$

Thus to understand, quantify and model this process, the change in thermal state, heat transfer condition ΔQ_{state}, materials expansion coefficients $\overline{\alpha_{L_i}}$ and/or nominal expansion $\overrightarrow{NDE_{A-B}}$ of metrology frame have firstly to be experimentally evaluated [21].

The change of the thermal field ($\overrightarrow{\Delta T_{field_i}}$) within an assembly component can be quantified by mixture a of heat loads measurements and modelling applying the equations of heat transfer. Simplified schematic of the assumed heat transfer analysis mechanism for solid assemblies can be seen in (Fig. 7).

There would be $a)i$ number of components that would in total experience positive change of increase of heat loads/Inputs ($\Delta Qini$) and thus surface area temperature ($\Delta Tface\ ini$). There would be $b)i$ number of components that would experience a general decrease of heat flow ($\Delta Qouti$) and thus surface temperature. There would be $c)i$ number of inter-component interfaces for which there will be internal heat transfer ($\Delta Qtransi$) and thus internal assembly faces change in temperature variation (Fig. 7). If all boundary changes (internal and external) of heat transfer are measured or calculated (refered as TL_i, with a statement of uncertainty- U_{TL_i}), the knowledge can be used to calculate the change in the assembly components thermal field. This in consequence can be used to calculate any change in internal stresses and thus dimensions of the assembly as function of the current mechanical constraints.

Currently, the best official reference defining such deformation evaluation procedures is an existing ISO technical report ISO/TR 16015 [21]. This work illustrates the significance of monitoring the thermal effects on measurand pieces and the importance of evaluation and correction of any such systematic error are addressed. In this work, the measurand is considered as a single component and not as a complex assembly. ISO/TR 16015 [21] addresses the combined use of experimental deformation evaluation and basic arithmetic calculations to quantify the thermal effects as a worst case scenario during metrology. However, it does not discuss the implication of computational prediction models based on online thermal load measurements. It concludes that such techniques would be too complex and lacking a statement of uncertainty. However, in the case of CLIC, the measurands are hundreds of complex assemblies, dimensionally deforming during machine operation, upon which direct deformation measurement might be uneconomical and unfeasible. Thus knowing if mathematical compensations (based on heat load measurements as input to the models) are possible with a known and traceable uncertainty (in the μm range) would fill an important gap of knowledge.

Prediction for Nominal Differential Expansion (NDE) can be done via three different families of models: *Analytical*, *Numerical* or *Empirical* (based on virtual or experimental data). The literature review performed related to these family of models has not found a validated application with an accurate and traceable statement of uncertainty for the compensations made [5,26–29]. However, several state-of-the can

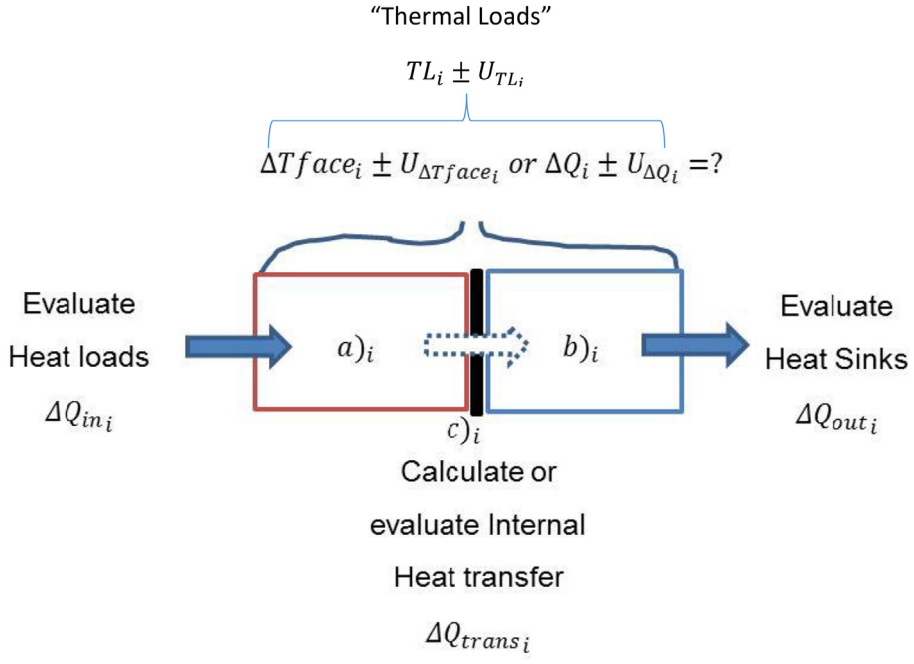

Fig. 7. Thermal loads boundary and internal conditions of assembly.

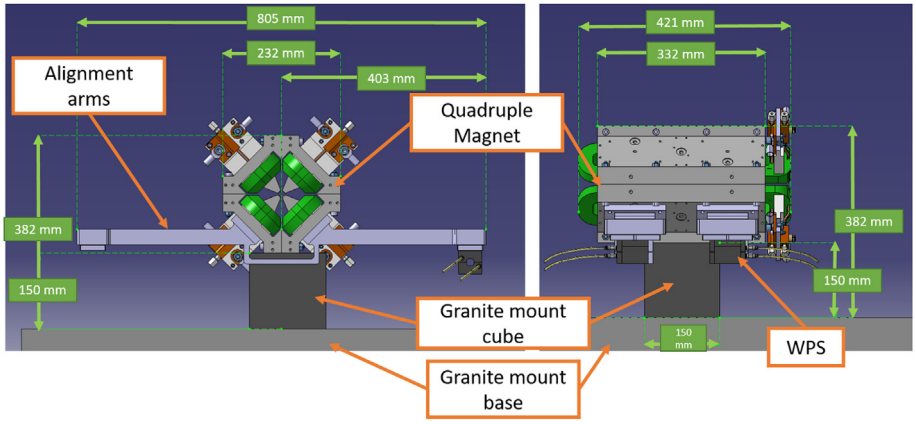

Fig. 8. Simplified prototype for studies, Left: Front view, Right: Side view.

be seen working in a similar direction, acknowledging the common challenge of thermal deformation and metrology of large assemblies. Research done [27] for the Light Controlled Factory EU project [30] has shown how online thermal measurements can be mixed with FEM for compensation thermal deformation. However, a lack of uncertainty evaluation of the FEM modelling has been observed. In the same work, it was discussed as a possible line for future research. Work performed for Herschel-Space observatory [26] and research at the National Institute of Standards and Technology USA (NIST) for virtual FEM Metrology [29] have shown the potential of Probabilistic FEM for quantification of model outputs sensitivity to the uncertainty of input parameters. However, the approach has not been observed applied and validated for real assemblies deformation prediction with associated uncertainty.

Studying the literature, gaps of knowledge and work on the PACMAN project has defined the following hypothesis which is further studied and verified by the current work:

Thermal deformations can be predicted accurately by models with known uncertainty of the prediction that being a function of measured model bias [ε] *and estimated model variability* [$V(x)^{1/2}$] - *a function of model input parameter standard uncertainties.*

Due to the high assembly complexity of CLIC (Fig. 3) assembly modules, it was decided to design and manufacture and assemble additional simplified prototype that can still serve as proof of concept (Fig. 8) but with lower complexity.

The simplified assembly was formed by striping all necessary auxiliary equipment and leaving only essential for the studies magnet Steel yokes, Aluminium 'alignment arms' [referred also as 'Beam (Aluminium)' in Fig. 2] and Copper coils. The complete assembly was supported on the metrology granite CMM table via granite cube eliminating any possible influences due to the 5 dof high precision alignment system. In the current paper modelling and experimental studies are related only on the 'simplified' magnet prototype Fig. 8 having dimensions of its metrology frame similar to 'T1' (Fig. 3).

The simplified prototype was studied both inside CERN accelerator tunnel laboratory (Fig. 9 A)) and inside Leitz Infinity CMM system at CERN Metrology Laboratory (Fig. 9 B)). Thermal Load Sensors (TLS) were installed among and around the magnet assembly. By thermal load sensors, we imply a combination of heat-flux chip, surface and air mounted temperature sensors [31–33]. A combination of those were installed on each of the assembly sub-components faces – side, top bottom. TLS were installed as well on the granite mount cube, granite mount base and water thermal control system Inlet and outlet.

As an alternative to the CMM measurement, a WPS system [12,13] with stretched carbon fibre wire (stable location reference) was utilized as an alternative independent system that can measure the NDE between a stretched wire and a sensor in the micron level uncertainty. Reference precision spheres fiducials were permanently glued to the surface of the quadruple magnet, alignment arms, granite cube and granite mount base. Each sphere was measured, and it's centre defined by the CMM used for the NDE evaluation. The spheres used were 6 mm diameter stainless steel ball bearings of Class 3 (ISO-3290) with a maximum out of roundness error of 1 μm. They were permanently glued compressing them toward the metal face with a thin layer of Araldite® epoxy glue with CTE of $90 \times 10^{-6}\ K^{-1}$.

Following the initial location measurements, the thermal loads on the assembly were varied via a combination of water chiller thermal control system [34] and air fan as shown in Fig. 9. The temperature state of the assembly was thermally stabilized at various steady states differing from the state at which the initial alignment measurements were taken in the range of ± 10 °C (mean temperature of the magnet faces). A vibrating stretched wire magnetic measurement system [35–37] was used to best-fit the wire at the magnet axis correspondent for each studied thermal equilibrium state away from the initial alignment one. The absolute location of the reference stretched wire was measured at each such instance from a separate set of WPS sensors mounted directly on the assembly Fig. 9. The data from the tunnel experiments (Fig. 9 A)) was used for the creation of Empirical (3.1), PFEM (3.2) and Meta-model based on PFEM (3.3). The experiments were then repeated within the metrology laboratory where WPS system was used for bias 3 estimation of the prediction models and the CMM system was used as independent means for validation of the model's prediction (Fig. 9 B)). The WPS system was decided as an adequate device for measurement of model bias due to its low and traceable to the metre measurement uncertainty [12].

3. Methodology proposed

Every measurement (or prediction) error can be split in two main general categories, systematic and random. Measurand uncertainty as defined by the Guide to the Expression of Uncertainties GUM [16,38] is a function of the complete measurement (or modelling in the current case) process variability being combined with the systematic unknown/uncorrected but accounted for errors. The standard relies on the fact that all understood systematic errors are quantified and corrected, and if not corrected they are accounted for in the standard uncertainties part of the budget. If we accept that the prediction of Nominal Differential Expansion ($\overrightarrow{NDE}$) by the use of a model (Empirical, FEM or FEM Meta-model) is a form of 'virtual measurement', we can estimate its uncertainty by following GUM (Supplement 1) methodology [16] quantifying its prediction standard deviation [$V(x)^{1/2}$] and its bias from the true values (Fig. 10).

Following the suggested method, a probabilistic version of the prediction model (being Empirical, FEM or a FEM based Meta-model) is performed by propagating the uncertainty in each of the model control parameters to its final output following Monte-Carlo based sampling.

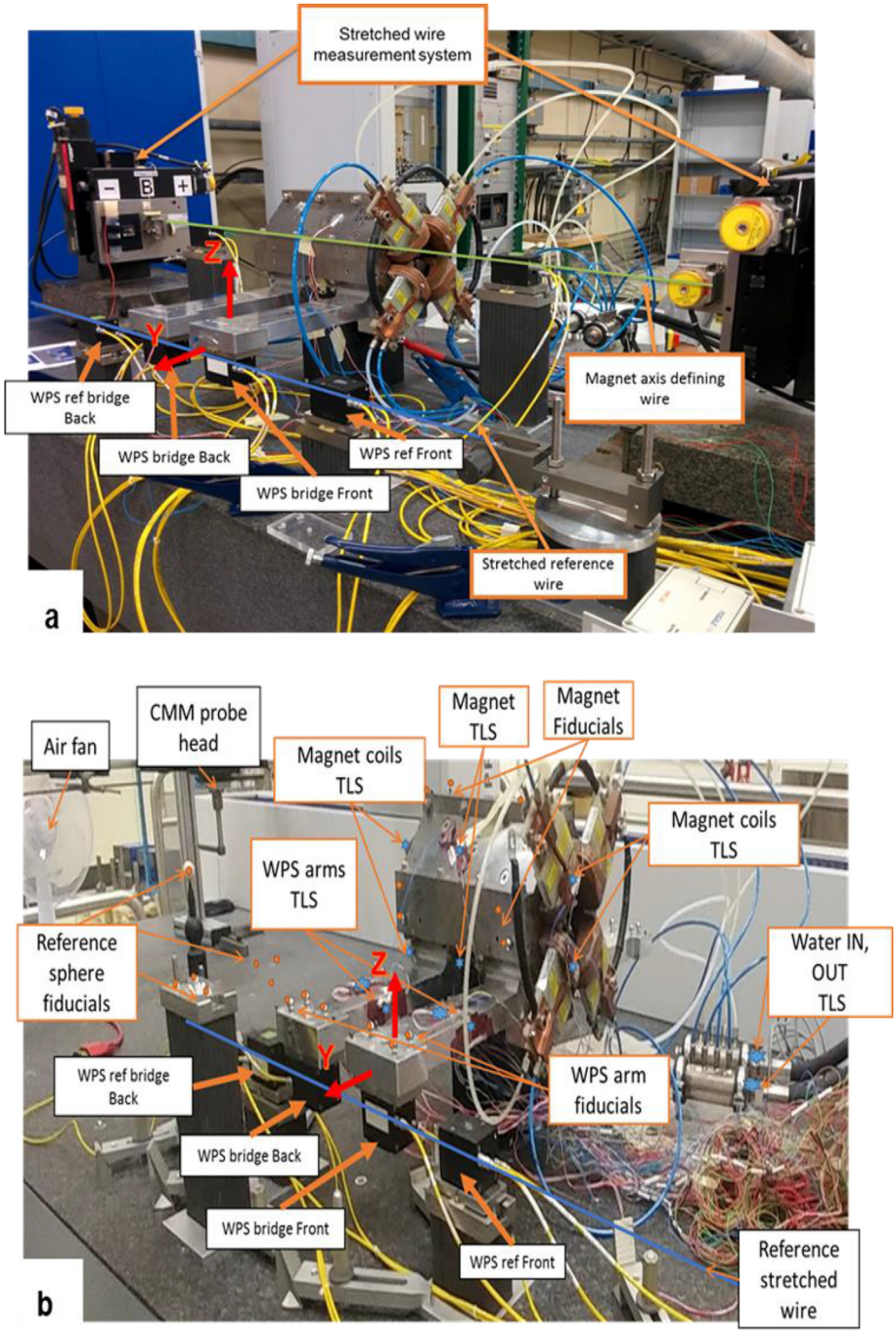

Fig. 9. A) Experimental setup for gathering data of Nominal Differential Expansion of Magnet axis with respect to alignment reference (used for empirical regression model creation) B) Experimental setup for CMM validation measurements of model predictions.

For the empirical model a direct Monte-Carlo on a regression model (based on Thermal Loads TL_i and drift measurements NDE_{A-Bi}) was performed for the variability study. For the FEM and it's meta-models 'Design of Experiments' [39], 'Latin Hyper Cube' [40–42] and other efficient sampling and 'design space' studying techniques combined with High-Performance Computing grids [43] were applied. The variability of the output of such a probabilistic model could be accepted as the model uncertainty according to GUM Supplement 1 standard. This as long as the model is 'perfect', with zero bias and mean-variance from the true value. However, no matter how precise models are they would always include bias from reality which has to be quantified and added to the uncertainty statement. To quantify a measurement or model bias, a reference to a true or so-called 'conventional true value' must exist. For thermal deformation, the true value can be accepted as the real deformation of an assembly of interest. Thus an reference calibration experiment with sufficiently small, known and tracable statement of uncertainty must be performed. Thus comparing the real measured deformation to the one predicted by the 'virtual model'. Finally, the uncertainty of the prediction model can be defined as a function of the measured *Bias* and the modelled *Variability* (Eq. (8)).

$$U_{NDEmodel} = f\,(Bias + \ Variability) \tag{8}$$

This methodology is further expanded for Empirical, FEM and FEM meta-models in following paragraphs **3.1**, **3.2** and **3.3**.

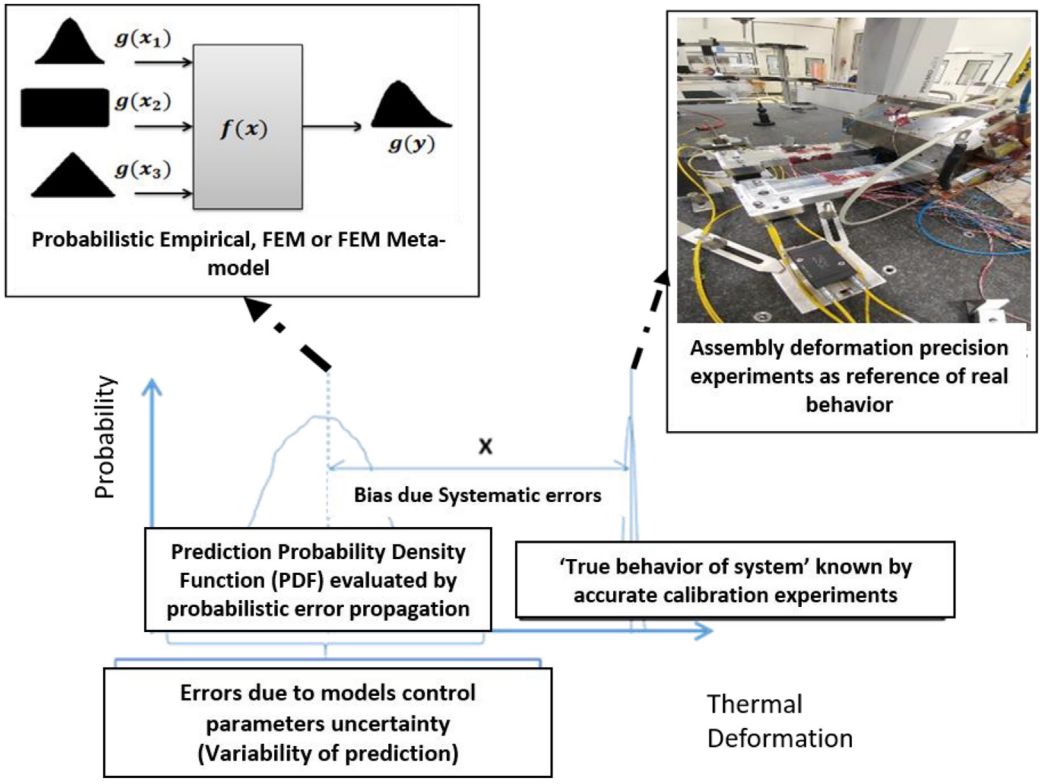

Fig. 10. Deformation model uncertainty estimated by a mixture of probabilistic modelling for model standard deviation estimation and comparison to real assembly thermal behaviour for model bias estimation.

3.1. Estimation of the empirical model's prediction uncertainty

The uncertainty of any empirical model prediction is assumed to be related to the extrinsic uncertainty of the experimental measurements used for its creation $U_{NDE_{A-B\,i}}$, U_{TL_i} and the *bias* (ε_{emp}) of its performance representing the true value. The complete process is visually represented in (Fig. 11).

The prediction uncertainty of the empirical model was defined as the empirical model variability [$v = f(P^T(TL_i), \hat{\beta})$] directly summed to its uncorrected bias ε_i (Eq. (9)). This direct bias adding concept was first defined as the 'SUMU method' in Ref. [44] and in this work applied in the field of uncertainty propagation for empirical models.

$$U_{\widehat{NDE_{A-B}(TL_i)}} = f(v,\ \varepsilon_{emp}) = f(P^T(TL_i), \hat{\beta}) + \varepsilon_{emp} \tag{9}$$

where $P^T(TL_i)$ is the polynomial basis function (of the thermal loads in this case),

$$P^T(TL_i) = [1\ TL_1 TL_2\ TL_3 ... TL_1^2 TL_2^2 TL_3^2 ...\ TL_1 TL_2\ \ TL_1 TL_3 ...\ TL_2 TL_3 ...] \tag{10}$$

and $\hat{\beta}$ is a vector containing the unknown regression coefficients. These coefficients were estimated from the measured sample set of NDE_{A-B_i} and TL_i. By using matrix notation, the resulting vector of estimated regression coefficient was as defined in Eq. (11).

$$\hat{\beta} = (P^T P)^{-1} P^T \overrightarrow{NDE_{A-Bi}} \tag{11}$$

Where ?? is the matrix containing the basis polynomials for the evaluated thermal samples/measurements TL_i and $\overrightarrow{NDE_{A-Bi}}$ is the vector of the measured/evaluated experimentally drifts.

In Eq. (9) ε_{emp} the bias between the true value and the predicted one by the empirical model. This can be estimated by high accuracy

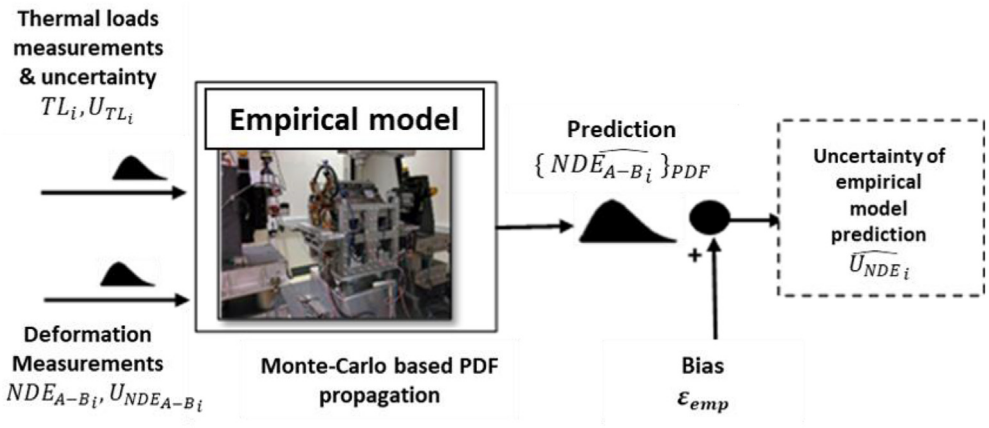

Fig. 11. Flowchart expressing the uncertainty of empirical model prediction as sum of its prediction variability and bias flowchart.

measurment with known and tracable statement of uncertainty providing the reference to a true value. In the current campaign, the regression model was created by measurements made with a WPS high precision metrology system [12,13], at various thermal gradients within CERN underground tunnel laboratory (Fig. 9 A)). The empirical model bias was then evaluated by the same WPS measurement system but within CERN Metrology laboratory at similar but not identical steady state thermal conditions – (not exact airstream and temperature condition and chiller set temperatures - Fig. 9 B)). The WPS measurements were with pre-establish uncertainty $U_{NDE_{A-Bwps}}$. Thus, the bias error was estimated with respect to the worst possible case ($NDE_{A-B} \pm U_{NDE_{A-Bwps}}$) adding the (1σ) uncertainty toward the validation measurment. The bias was defined as the maximum measured difference between the mean of the empirical model prediction PDF and the validation measurment with it's added uncertainty (Eq. (12)).

$$\varepsilon_{emp} = \max_{NE} \left| \left(NDE_{A-B_i} \pm U_{NDE_{A-B_{wps}}}\right) - \mu_{\{\hat{NDE}_{A-B_i}\}\{\hat{NDE}_{A-B_i}\}_{\boldsymbol{PDF}}} \right| \quad (12)$$

The variability $v = f(P^T(TL_i)\hat{\beta})$ of the Empirical model, was estimated via Monte-Carlo method by propagating the uncertainty of $P^T(TL_i)$ and β as a function of the measurement uncertainties used for their definition via the regression analysis:

$$U_{P^T(TL_i)} = f\left(U_{TL_i}\right) \text{and} U_{\hat{\beta}} = f\left(U_{TL_i}, U_{NDE_{A-B_i}}\right) \quad 13)$$

The U_{TL_i}, $U_{NDE_{A-Bi}}$ were experimentally evaluated [14] for the sensorial systems used. From their PDFs, random sampling (300 000 iterations) was performed and the sampled values were propagated through the complete regression model for the evaluation of $P^T(TL_i)$, $\hat{\beta}$ and thus the regression model iteratively. Thus the empirical model output $\hat{NDE}_{A-B_i}$ was described by the realisations PDF (Fig. 11) with mean - $\mu_{\{\hat{NDE}_{A-B_i}\}\{\hat{NDE}_{A-B_i}\}_{\boldsymbol{PDF}}}$ representing the most likely value and a variability - $S_{\{\hat{NDE}_{A-B_i}\}\{\hat{NDE}_{A-B_i}\}_{\boldsymbol{PDF}}}$ represented by the standard deviation of the prediction. The nominal deformation prediction variability (scaled by the coverage factor k = 1,2 or 3) summed with the measured (during model validation) bias ε_i provided the statement of uncertainty for the Empirical model for this particular assembly and thermal load ranges (Eq. (14)).

$$U_{\hat{NDE}_{A-B_i}} = \left(k * S_{\{\hat{NDE}_{A-B_i}\}_{\boldsymbol{PDF}}}\right) + \varepsilon_{emp} + \varepsilon_{emp} \quad (14)$$

3.2. Estimation of FEM models prediction uncertainty

The procedure for evaluation of FEM predictions ($\hat{NDE}_{A-Bi}$) and uncertainty ($U_{\hat{NDE}_{A-B_i}}$) was defined following the same methodology: the mixed approach of Probabilistic FEM (for model variability estimation) and model bias evaluation (by experimentation). The FEM based error compensation approach is more flexible than the Empirical modelling as, once validated, it can be used to predict nominal expansion with associated uncertainty for condition ranges outside the ones performed experimentally. A visual summary of the method can be seen in Fig. 12.

The initial step was the creation of a thermo-mechanical FEM model. The model was created in ANSYS FEM software using the 3D manufacturing models of the components. Mechanical constraints were set exactly as those for the real assembly. The boundary conditions – thermal loads (TL_i), material expansion coefficients (α_{L_i}), internal and external for the assembly heat transfer coefficients ($\hat{HTC}_i$) were set to those measured during alignment calibration experiments. The next step was to parametrise the FEM model and to link ANSYS and Dynardo [43,45] statistical software, thus, performing probabilistic FEM modelling. In this way, the input parameters were defined as Probability Density Functions (PDF) which quantify the uncertainty in their knowledge. These PDFs were iteratively sampled and propagated through the FEM model acting as a 'virtual experiments' similar to state-of-the-art work presented in Refs. [39,46]. This step was achieved by applying the Latin Hyper Cube technique in order to reduce the sample size for the computationally expensive FEM model. Only a few hundred (~250) FEM model iterations were required [47] for achieving a probabilistically significant result for the $\{\hat{NDE}_{A-B_i}\}\{\hat{NDE}_{A-B_i}\}_{\boldsymbol{PDF}}$ via this approach. High Performance Computing (HPC) was used for performing the iterations in parallel on separate cores, processors and servers as suggested by Ref. [43] in order to reduce and optimise computation time and costs. The output from the numerous iterative FEM simulations ('virtual experiments') formed a PDF with associated mean ($\mu_{\{\hat{NDE}_{A-B_i}\}\{\hat{NDE}_{A-B_i}\}_{\boldsymbol{PDF}}}$) and variability ($S_{\{\hat{NDE}_{A-B_i}\}\{\hat{NDE}_{A-B_i}\}_{\boldsymbol{PDF}}}$). The mean of the output PDF was accepted as the most likely nominal expansion prediction according to the model. Following this, the bias of the Probabilistic FEM model was evaluated by comparing its mean to the traceable to the metre accurate measurements of deformation performed by 2x independent systems – a CMM and a WPS (each with known uncertainty $U_{NDE_{A-B\,cmm\ or\ wps}}$). The validation measurements were acting as a reference to the real Nominal Differential Expansion (NDE). The bias error was estimated with respect to the worst possible case which is the direct sum of the NDE measured and its measurment uncertainty ($NDE_{A-B} + U_{NDE_{A-B}^{cmm\ or\ wps}}$) (Eq. (15)).

$$\varepsilon_{\text{FEM}} = \max_{NE} \left| \left(NDE_{A-B_i} \pm U_{NDE_{A-B}^{cmm\ or\ wps}}\right) - \mu_{\{\hat{NDE}_{A-B_i}\}\{\hat{NDE}_{A-B_i}\}_{\boldsymbol{PDF}}} \right| \quad (15)$$

The final prediction uncertainty of the Probabilistic FEM was evaluated following the 'SUMU method' for summation of uncorrected bias as first defined in Ref. [44] (Eq. (16) and Fig. 12).

$$U_{\hat{NDE}_{A-B_i}} = \left(k * S_{\{\hat{NDE}_{A-B_i}\}\{\hat{NDE}_{A-B_i}\}_{\boldsymbol{PDF}}}\right) + \varepsilon_{\text{fem}} \quad (16)$$

An alternative to this approach would be to account for the measurement bias within the probabilistic (Mote-Carlo) variability study by considering the output results a bi-modal distributed variable with peaks at + or – the bias value. In the current paper however the 'SUMU method' was used.

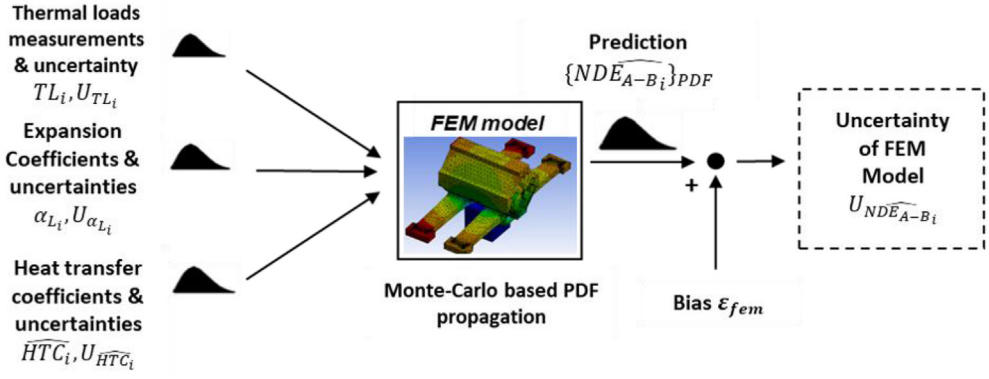

Fig. 12. Uncertainty propagation of a FEM model as sum of its prediction variability and bias flowchart.

With the current procedure, predictions with associated uncertainty were performed in non-real-time. Even a highly optimized HPC system failed to provide even near-real-time computing due to the required several hundred computationally intensive FEM iterations. Thus, such studies could be used only a priori to any actual effect for studying the expected performance with known uncertainty. As near or real-time compensation results in uncertainty statements (based on Probabilistic FEM) were required, an additional sub modelling procedure (meta-modelling [48]) was prepared in advance, creating a simplified analytical model based on the FEM studies. This procedure is detailed in the next section.

3.3. Estimation of the FEM meta-models prediction uncertainty

The concept behind meta-modelling is to use the FEM instead of the real assembly as the transfer function for the propagation of input parameters (thermal heat transfer loads) to output responses (Nominal Differential Expansions). Thus, the measured thermal loads (TL_i) and the output results ($\hat{NDE}_{A-B\,i}$) of the FEM were used to create an analytical 'meta-model' by applying regression analysis. In this way, the empirical model is solely based on 'virtual experiments' being the FEM simulation rather than real experiments. This provided an analytical equation (the meta-model of the FEM) that predicts Nominal Differential Expansion ($\hat{NDE}_{A-B\,i}$) as function of measured (TL_i). The uncertainty of the meta-model was propagated following the same procedure designed for the empirical model's uncertainty analysis. Thus, the meta-model uncertainty was devised to be a function of the thermal load measurements PDF described by their uncertainty's (U_{TL_i}) and the Probabilistic FEM model prediction PDF (described by its modelled uncertainty ($U_{\hat{NDE}_{A-B_i}}$)) as shown in Fig. 13.

Those were propagated via the Monte-Carlo method though a regression analysis procedure in the same way as for the empirical measurement models **3.1**. The output of the probabilistic propagation is an output PDF of the meta-model with associated mean ($\mu_{\{\hat{NDE}_{A-B_i}\}\{\hat{NDE}_{A-B_i}\}_{\boldsymbol{PDF}}}$) and variability ($S_{\{\hat{NDE}_{A-B_i}\}\{\hat{NDE}_{A-B_i}\}_{\boldsymbol{PDF}}}$). The mean of the PDF prediction for the meta model was then validated against the calibration prediction made by the Probabilistic FEM (with uncertainty $U_{\hat{NDE}_{A-B_i}}$). This was used as a virtual reference defining the best knowledge of the assembly expansion. The bias error was estimated with respect to the worst possible case, which is the direct sum of the validation PFEM prediction and its' evaluated uncertainty ($\hat{NDE}_{A-B_i} + U_{\hat{NDE}_{A-B_i}}$), (Eq. (17)).

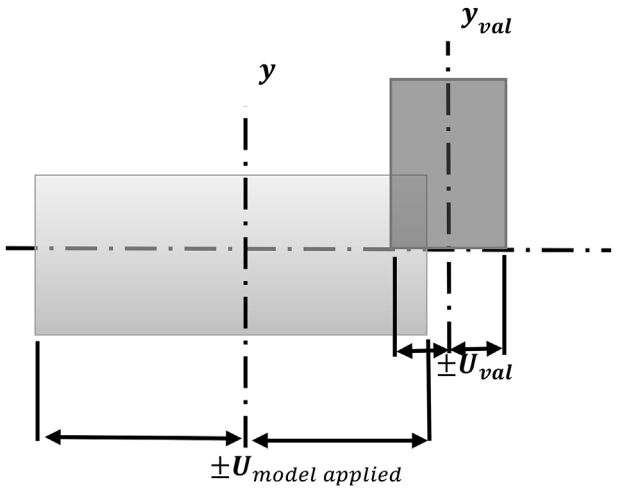

Fig. 14. Combining Uncertainty regions of the model applied and of the validation measurement [42].

$$\varepsilon_{\text{meta model}} = \max_{NE}\left[\left(\hat{NDE}_{A-B_i} + U_{\hat{NDE}_{A-B_i}}\right) - \hat{NDE}_{A-B_i}\right] \tag{17}$$

The final prediction uncertainty of the meta-model was finally estimated as a function of its propagated variability ($S_{\{\hat{NDE}_{A-B}\}\{\hat{NDE}_{A-B}\}_{\boldsymbol{PDF}}}$) and evaluated bias ($\varepsilon_{\text{meta model}}$) (Eq. (18) and Fig. 13).

$$U_{\hat{NDE}_{A-B_i}} = \left(k * S_{\{\hat{NDE}_{A-B_i}\}\{\hat{NDE}_{A-B_i}\}_{\boldsymbol{PDF}}}\right) + \varepsilon_{\text{meta model}} \tag{18}$$

3.4. Validation procedure for prediction of model uncertainty accuracy

The final step for Empirical, FEM, and Metamodels was a validation of their predictions and statements of uncertainty. This was done following suggestions from Ref. [49] by comparing the model's outputs (*Ymodel applied*) and their predicted uncertainty zones ($U_{model\ applied}$) against real experimental data (*Yval*) measured with low uncertainty

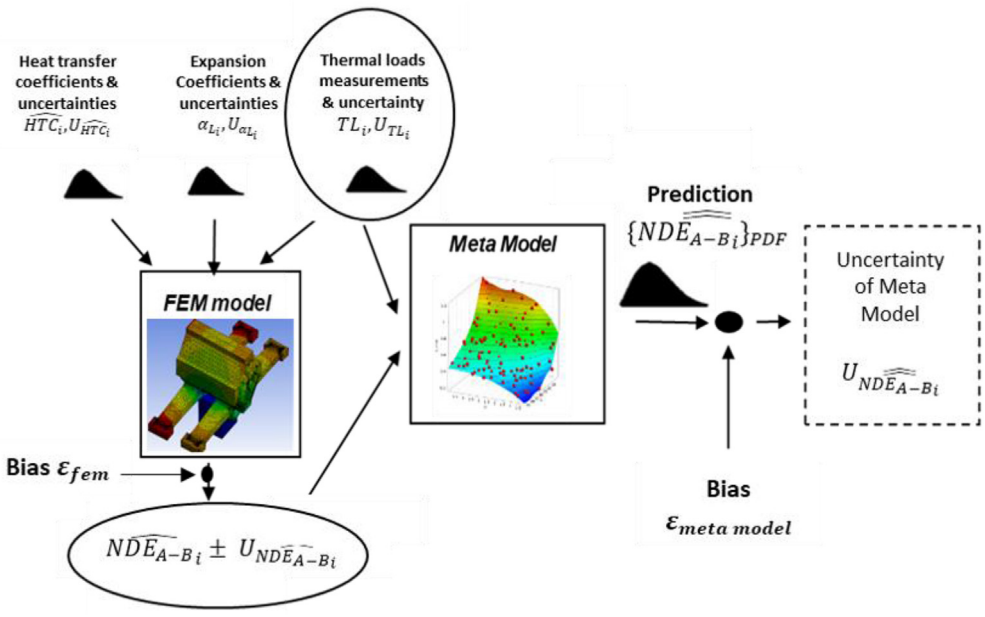

Fig. 13. Uncertainty propagation of a Meta-Model being a sum of its prediction variability and the validated bias flowchart.

Table 1
Magnet axis location shift and temperature measurement uncertainties VS empirical model variability, bias and standard combined prediction uncertainty.

Calibration measurements uncertainties 1s; Rectangular shape		Empirical model shift prediction		
U *magnet axis shiftmeasurment* /μm	U *thermal load measurment* /°C	$S_{N\hat{D}E\hat{Z}}$/μm	$\varepsilon_{N\hat{D}E\hat{Z}}$/μm	$U_{N\hat{D}E\hat{Z}}$ 1s/μm
3.56; a = 6.17	0.182; a = 0.32	3.08	6.49	9.57

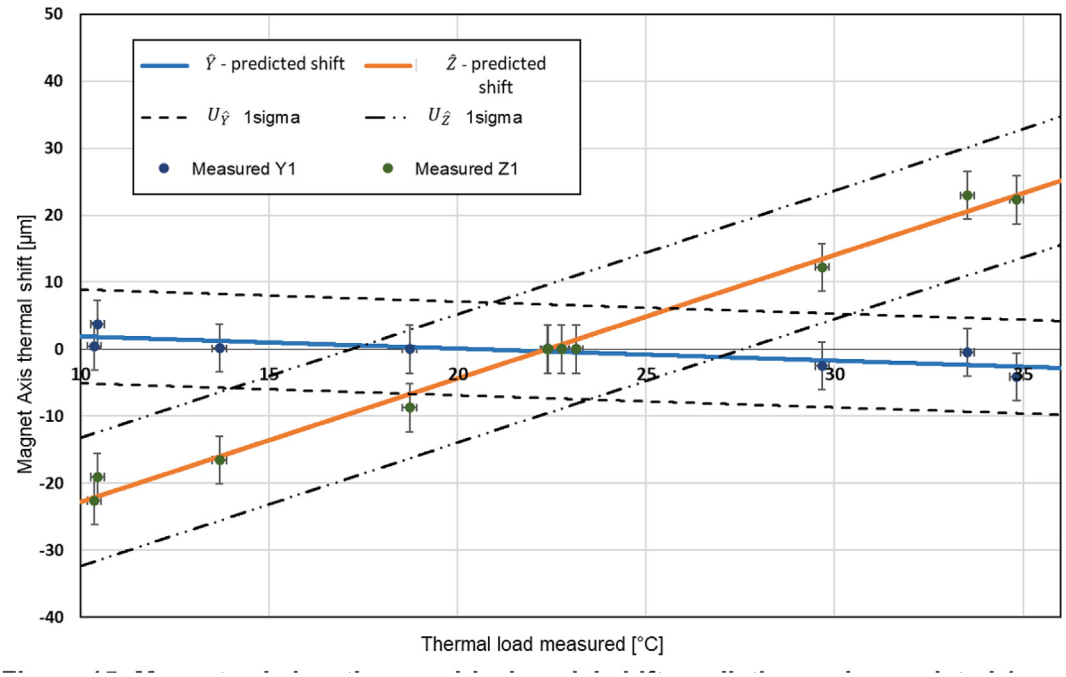

Fig. 15. Magnet axis location empirical model shift prediction and associated 1σ uncertainty of the prediction VS validation measurement samples and their 1s standard uncertainty.

U_{val} as shown in Eq. (19) and Fig. 14.

$$En = \frac{Ymodel\ applied - Yval}{\sqrt{Uval^2 + Umodel\ applied^2}} \leq 1\ \text{Yes(pass) or No(fail)?} \tag{19}$$

where *Ymodel applied* is the prediction of a model (PFEM, empirical or meta-model) calibrated with known bias estimated experimentally by WPS system and *Yval* is high precision independent from the bias calibration reference measurement of the thermal deformation (made via Leitz Infinity CMM [50,51]). By this (Eq. (19)), if the result is less than 1, it can be considered that the validation measurement was within the predicted uncertainty region and thus the uncertainty region of the model is being predicted correctly (Fig. 14). If the test (Eq. (19)) is not passed, then the method fails to predicts accurately the uncertainty region.

4. Results

In this section, the results from two empirical models (for magnetic axis **4.1** and fiducials **4.2**) and two FEM based models (probabilistic FEM and FEM meta-model both for fiducials) of thermal deformation/shift effects are outlined.

4.1. Uncertainty of empirical model prediction for magnet axis thermal shift

In Table 1 the input measurement uncertainties for the probabilistic analysis of the empirical model (as related to 'WPS bridge front' in Fig. 9, **B)** Z direction) and the output results for the model prediction variability $S_{\hat{Z}}$ and bias ε_Z are shown. The final combined uncertainty for the empirical prediction $U_{\hat{Z}}$ is also shown. From all the experimental data available, a probabilistic correlation analysis of input versus output responses was performed to estimate the most influential thermal loads for the magnetic axis shift prediction. For the current study, the mean value of the magnet yoke temperature was the most influential for the magnet axis shift behaviour [14]. Thus, an assumption was made to base the magnetic axis empirical model on the mean of all magnet yoke installed sensors referred to as 'thermal load measurement' in the figures below.

Where the total prediction $U_{\hat{Z}}$ uncertainty was calculated via the Root Sum of the Squares The uncertainty summation (RSSU) method (considering the bias and variability as uncorrelated entities) is defined in Ref. [44]. Only Z direction results are shown as most representative for the largest uncertainty at 1*s* for the empirical model. In Fig. 15 one can observe the predicted behaviour of the magnetic axis thermal shift as a function to the mean magnet yoke temperature. The prediction is shown with its' 1*s* predicted uncertainty envelope. Reference measurements (with their uncertainties in 1*s*) of the real axis location are also shown in In Fig. 15.

4.2. Uncertainty of empirical model prediction for fiducials thermal shift

In Table 2 input (parameters uncertainties) and output (variability and bias) parameters results can be seen for the studied fiducial thermal shifts empirical model. The final combined prediction uncertainty for the empirical model in Y and Z coordinates: $U_{\hat{Y}}$ and $U_{\hat{Z}}$ is also shown. The uncertainty of the independent CMM validation measurement and the validation test coefficient are also outlined.

In Fig. 16 the CMM validation measurements and the WPS

Table 2
Fiducials location shift and temperature measurement uncertainty VS empirical model variability, bias and combined standard prediction uncertainty.

Calibration measurement uncertainties 1*s*; Rectangular shape	Thermal shift direction	$S(1s)$/μm	ε/μm	U 1*s*/μm	Validation measurement uncertainty (CMM) 1*s*/μm; Gaussian	Validation test coefficient w.r.t. (CMM)
20. $U_{fiducials\ shift}$ /μm $_{measurment}$	$\hat{Y}$	3.69	5.07	8.76	2.05	0.32
21. $U_{thermal\ load\ measurment}$ /°C 1.17; a = 2.05 0.26; a = 0.445	$\hat{Z}$	2.04	7.89	9.93	2.05	0.58

calibration measurements are shown with respect to the model, and it's standard uncertainty regions are represented.

4.3. Uncertainty of FEM and FEM-based metamodels prediction for fiducials location shift

The thermal load measurements from various heat-flux, thermal probes and thermal radiation camera sensors were taken and used as input to a FEM model. Images of the experimental setup and a visualization of a single stress calculation of the corresponding FEM can be seen in Fig. 17.

In Fig. 18 the same data is represented visually showing the Probabilistic FEM prediction as the mean of its PDF and its estimated uncertainty (1σ). These are compared against validation measurements made from two independent metrology tools – CMM and WPS stretched wire systems.

An analytical metamodel based on FEM prediction was created, and its uncertainty was studied following the procedure and method defined. Results can be seen summarised in Table 5.

5. Discussion

The studies and results for the thermal errors size the expected uncertainty with which they can be compensated have shown the importance of addressing thermal effects in a detailed manner. Frequently missed in uncertainty budget for alignment measurements, thermal errors and the uncertainty of any compensations applied can be critical for high precision alignment. The results showed that thermal effects post-metrology could shift the magnetic axis location by dozens of μm and alignment features by hundreds of μm and more. Thus, for high precision applications, not only accurate alignment metrology is important but also precision compensation for any post-metrology thermal effects. Although thermal compensation by the use of models has been performed on many occasions in state-of-the-art works [22,23,28,52–54], no statements of uncertainty validated and traceable to the metre standard have been found.

In the current work, following the hypothesis suggested, a successful evaluation of the prediction model's uncertainty was made. This was done by a combination of their evaluated Bias and Variability of prediction as defined in **3.** The hypothesis suggested in this paper was validated for Empirical Table 2, Probabilistic FEM Table 4 and Metamodels Table 5. Validation was agreed as independent CMM measurements were overlapping sufficiently with the predicted standard uncertainty regions for the three types of models. An outline of the evaluated models variability's, biases and combined prediction uncertainty for the different thermal error compensation models can be seen in Fig. 19.

It is important to outline that in the current studies; model bias is a predominant component of the prediction uncertainty. An exception to that observation is the Probabilistic FEM (PFEM) model and results for Y direction of fiducials thermal shift (Fig. 19). In this particular model, the shift in Z direction had a systematically larger bias error (Fig. 18). The larger bias errors can be explained by complexity in modelling accurately the thermal deformations for such assemblies' structures. This is believed to be due to inaccuracies in modelling the assembly interfaces behaviour and mechanical constraints. For these, a number of assumptions and simplifications were made in order to reduce the computational cost, such as bonded instead of frictional bolted contacts. For the empirical models, the large bias errors observed can be explained due to the difference between the thermal conditions at calibration and those when the model was applied. The further thermal conditions during machine operation deviate from those at model calibration, the larger would be the bias error of such a model. In our experiments, such deviations did exist as the thermal loads at the tunnel and metrology laboratory were not recreated identically. This is an expected limitation of empirical models.

Table 3
FEM Models significant Input parameters and their associated standard measurement uncertainties. In Table 4 the corresponding results of studding Probabilistic FEM model uncertainty can be seen for two fiducials part of the studied magnet assembly.

Input Parameter Class	Mean Values ranges for class	***S*** (standard measurement uncertainties)/1s	PDF shape
CTE coefficients of materials/ (μm/m °C)	From **6.9** (Granite base) to **24.2** (Aluminium WPS arm)	From **1.05** (Granite) to **0.44** (Steel of magnet Yokes)	Rectangular shape
Convection coefficients (forced convection) /(W/m^2 °C)	**10.67** (furthest away from air flow facing wall on WPS arms) to **35.33** (closest to air flow facing directly face of WPS arms)	From **0.65** to **2.11** (calibration certificate accuracy = 6% of Heat – Flux sensors reading value)	Rectangular shape
Emissivity coefficients/ε	**0.172** (Aluminium WPS arms) to **0.275** (Steel of Magnet)	**0.0078** to **0.07** (experimentally)	Rectangular shape
Temperatures measured/°C	**21.23** (Granite Base); **33.16** (Magnet inner faces at coils)	**0.05** (direct measurement at granite base) to **1.62** (extrapolation between magnet outer faces and coils measured temperatures)	Rectangular shape and Triangular biased

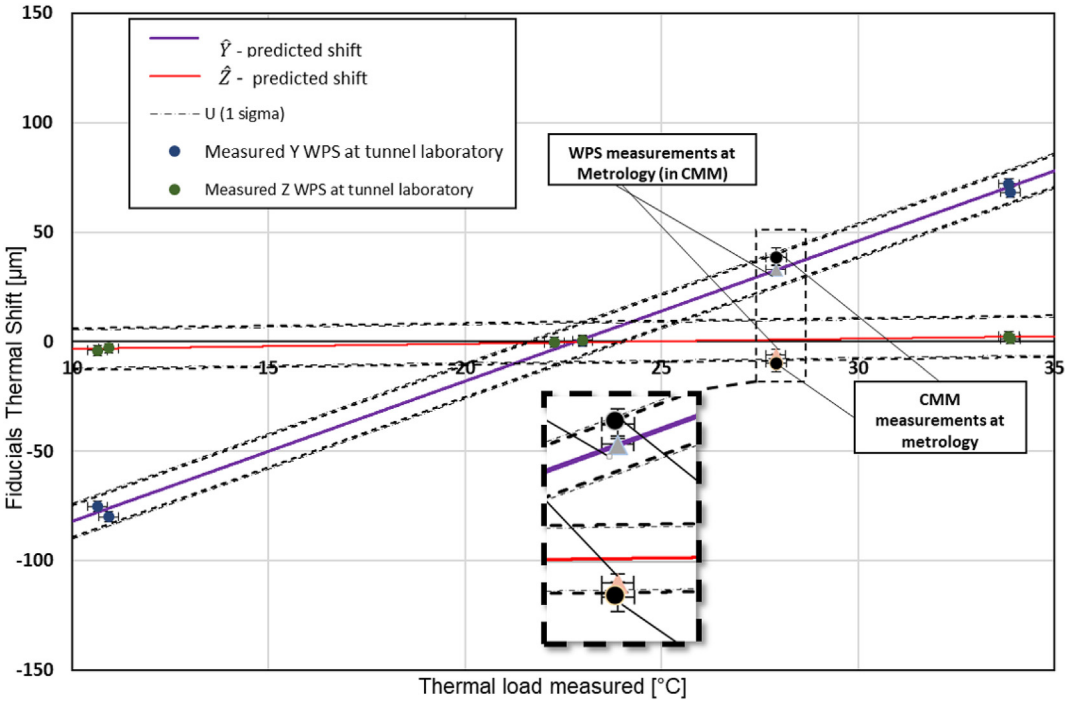

Fig. 16. Fiducials location shift empirical model prediction, associated standard uncertainty of the prediction VS measurement validation samples and their standard uncertainty.

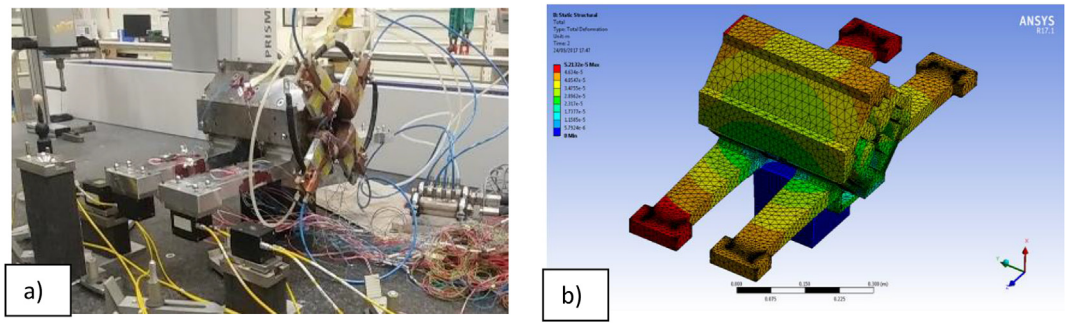

Fig. 17. a) Magnet assembly and WPS system integrated in CMM for thermal shift/deformation experiments; b) Total structural deformation FEM model single solution visual representation. A summary of the FEM model critical input parameters and their evaluated uncertainty can be seen in Table 3.

For conditions that are not economical or technically feasible to be studied experimentally in detail or for those that deviate from the existing data, numerical modelling is expected to be applied. As studied, accurately calibrated probabilistic FEM or Metamodel can be used with similar uncertainty of prediction ranges (Fig. 19). This statement is highly dependent on how well the FEM model and it's input parameters are calibrated and represents reality (size of the bias error). Applying Probabilistic FEM, one can not only learn the variability of the predictions but also evaluate which are the most sensitive parameters to the output variability via correlation-based analysis techniques [14,42]. For example, a small increase in the uncertainty of the CTE coefficients of the materials used could have a large impact on the variability of

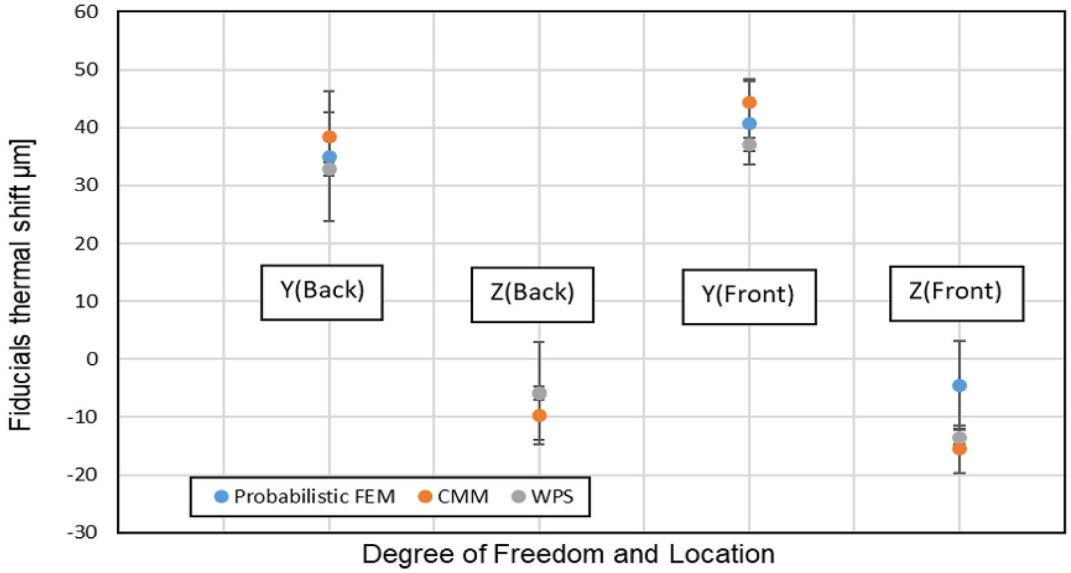

Fig. 18. A comparison between predicted (by Probabilistic FEM) fiducial shift with 1σ of prediction VS measured shift (by CMM and WPS) with 1*s* standard measurement uncertainties.

Table 4
Fiducials location shift probabilistic FEM parameters, associated uncertainty and validation parameters.

Magnet Assembly FEM					
Fiducials shift direction	Model Variability S 1s/µm	Model Bias/µm	Error (w.r.t CMM validation reading)/µm	Uncertainty 1s $U_{NDEassembly}$/µm	Validation (Test < 1 = PASS)
Y (back)	6.29	3.36	3.47	9.65	0.18
Z (back)	1.12	1.22	3.8	2.34	0.62
Y (front)	6.29	4.84	3.46	11.13	0.15
Z (front)	1.12	10.16	11.04	11.28	0.48

Table 5
Fiducials location shift metamodel parameters, associated uncertainty and validation parameter.

Magnet Assembly Meta Model FEM				
Shift direction	Model Variability S 1σ/µm	Model Bias/µm	Uncertainty 1s $U_{NDEassembly}$/µm	Validation Test < 1 = PASS
Y (back)	0.7	11.54	12.24	0.42

deformation/shift in location prediction and thus it's uncertainty [14,42]. In the same way, our studies revealed the importance of accurately knowing the heat transfer coefficients (such as air convection) for the various surfaces, which leads us to the additional use of heat flux sensors [14]. Such parameter probabilistic sensitivity studies can show the engineers which model parameters are most critical for the final prediction and, thus, worth resources for precise calibration.

It is important to note that without actual physical reference measurements, the bias error of a model cannot be determined and thus the true model prediction uncertainty neither. However, performing calibration measurements in a manner traceable to the metre can help to calibrate a Probabilistic FEM and FEM Meta-models to values close to the empirical counterparts.

This would imply that if once a numerical model is calibrated with minimized and known bias errors, it can be applied to any desired conditions with a known uncertainty statement. Thus, with a minimum number of experimental measurements, the designer can use the numerical based models to predict and compensate deformation behaviour for a wide band of conditions that might not be economically viable to be tested and represented by empirical measures. Moreover, one will be able to do this with a known and valid statement of uncertainty as shown in Table 2 Table 4 Table 5.

An additional property linked to empirical and metamodels being fitted to measurements or virtual measurements (FEM) is the 'variance bias trade-off error' [55–57]. The more complex function is used in order to fit best to the experimental data (with more control parameters), the larger would be the prediction variance [V(x)] and variability [$V(x)^{1/2}$] due to the more influential parameters contributing with their possible variance). The simpler a model is (two parameter polynomial), the less the variance error would be, but it would fit more poorly to the data and thus having a larger bias. This property can be used to make decisions on how complex empirical or metamodels should be, with respect to the measured bias errors.

For the Probabilistic FEM, the bias errors were one of our major limitations. For further improvement more effort on modelling the initial conditions, mechanical constraints represented by the model must be made. If all known and unknown bias errors are corrected, or taken as standard uncertainty contributors then the GUM Supplement 1 [16] scheme would apply completely (zero variance and bias of the mean), and the probabilistic model output variability would represent their ultimate standard uncertainties (a function of their calibration measurements uncertainties).

Uncertainty of model input parameters can have a big effect on prediction accuracy, furthermore, achieving near zero bias of models might not always be economically or technically possible. Thus, it is critical and important, as shown in the current work to distinguish and evaluate both model variability and bias. If this is done correctly, accurate statements of the prediction uncertainties can be made.

6. Conclusions and future work

In this work, a hypothesis and methodology were proposed as an

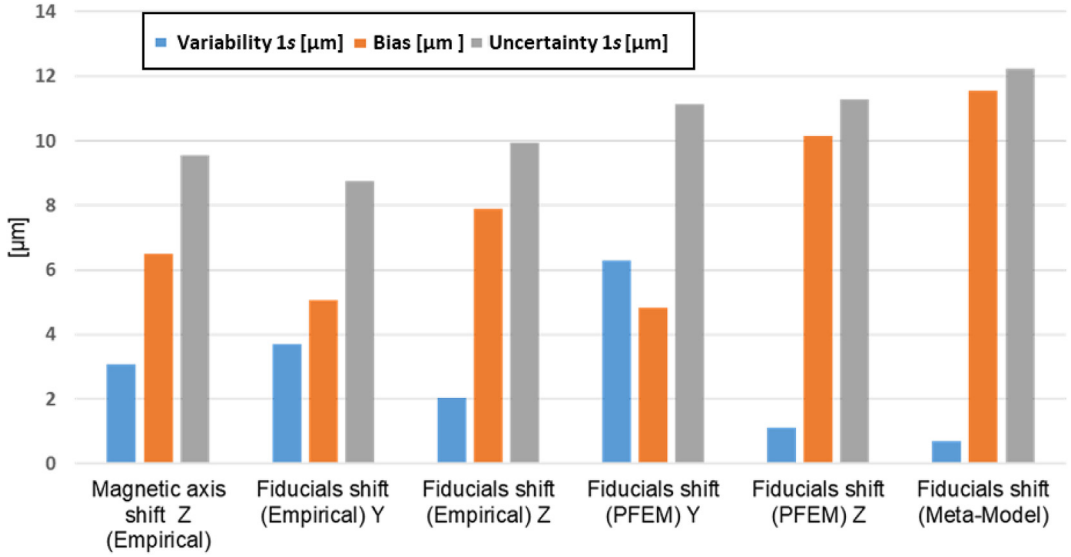

Fig. 19. Thermal error compensation models' variability, bias and combined uncertainty.

answer to the challenges in the CLIC project [9,58] of knowing the uncertainties due to thermal errors and their compensation made by models. It was shown that it is possible to deliver an accurate prediction of thermal shift with a valid statement of uncertainty. This was achieved by the mixture of: probabilistic modelling [16] for the evaluation of model variability and traceable measurements for the evaluation of model biases.

The proposed methodology was validated for our case study with respect to thermo-mechanical predictions. However, the idea could find practical applications in other fields of engineering and science where having an accurate uncertainty statement of model predictions is important. This could answer the need in industries such as aerospace and big science projects where uncertainty in predictions can have a high legal and financial impact. A direct example is a trend in state-of-the-art of having “digital twins” [59] models of critical systems. In parallel to system exploitation, a digital representative model is kept and fed with real-time data from the conditions under which the critical systems are subjected. Such models can be used to predict possible future behaviour (failure modes) or used as feedback to next-generation system design. The novel application of Machine Learning (gaussian models and Deep Neural Networks) for the creation of meta-models from FEM/CFD can be a fascinating and promising new line of research as shown in Refs. [60,61]. Such line could enable the creation of real-time high-fidelity digital twins (with known uncertainty) even for complex transient behaviour. Having accurate uncertainty statements of such predictions could help engineers in taking critical decisions. Thus, we believe that there is potential for this methodology to be further studied and validated in a wide band of possible application cases.

Acknowledgements

The research leading to these results has been coordinated by CERN and Cranfield University under the PACMAN project [62] framework. We would like to thank the people from the European Union for providing the financial support for the PACMAN project and for this current work in the form of the grant agreement PITN-GA-2013-606839 part of 7th Framework Programme, Marie Curie Actions. Special thanks as well to K. Doytchinov for his professional feedback, guidance, and support.

References

[1] Glassman T, Levi J, Liepmann T, Hahn W, Bisson G, Porpora D, et al. Alignment of the James Webb space telescope optical telescope element. In: MacEwen HA, Fazio GG, Lystrup M, Batalha N, Siegler N, Tong EC, editors. SPIE Astron. Telesc. - instrumentation. Int. Soc. Opt. Photonics International Society for Optics and Photonics; 2016. https://doi.org/10.1117/12.2233792.
[2] Slocum AH, Donmez A. Kinematic couplings for precision fixturing. Precis Eng 1988;10:115–22. https://doi.org/10.1016/0141-6359(88)90029-3.
[3] Stahl HP. Metrology of large parts. Handb Opt Dimens Metrol 2013:239–62.
[4] Arpaia P, Caiazza D, Petrone C, Russenschuck S. Performance of the stretched and vibrating wire techniques and correction of background fields in locating quadrupole magnetic axes. IMEKO World Congr; 2015.
[5] Bottura L, Buzio M, Pauletta S, Smirnov N. Measurement of magnetic axis in accelerator magnets: critical comparison of methods and instruments. IEEE instrum. Meas. Technol. Conf. Proc. Sorrento: IEEE; 2006. p. 765–70.
[6] Mainaud Durand H. Fiducialisation and initial alignment of the CLIC components within a micrometric accuracy. 14th Int. Work. Accel. Alignment. 2016.
[7] Mainaud Durand H, Touze T. The active pre-alignment of the CLIC components. 9th international workshop on accelerator alignment. Stanford, USA, Stanford, USA: 9th Int. Work. Accel. alignment; 2006.
[8] Doytchinov I. Alignment measurement uncertainties for large assemblies using probabilistic analysis techniques. University of Cranfield; 2017.
[9] CLIC (Collaboration). A Multi-TEV linear collider based on CLIC technology conceptual design report 2012. https://doi.org/10.5170/CERN-2012-007. Geneva.
[10] Mainaud Durand H, Artoos K, Buzio M, Caiazza D, Catalán Lasheras N, Cherif A, et al. PACMAN project: a new solution for the high-accuracy alignment of accelerator components. 2016. https://doi.org/10.18429/JACOW-IPAC2016-MOOCB01. MOOCB01.
[11] Caiazza D. Metrological performance enhancement of wire methods for magnetic field measurement in particle accelerators [PhD Thesis]. University of Sannio; 2017.
[12] Herty A. Test and calibration facility for HLS and WPS sensors vols. 4–7. 2004.
[13] Wire position sensor. 2017http://www.opensourceinstruments.com/WPS/, Accessed date: 14 August 2017.
[14] Doytchinov I. Alignment measurement uncertainties for large assemblies via probabilistic modelling techniques [PhD Thesis]. Cranfield University; 2018.
[15] Doytchinov I, Tonnellier X, Shore P, Modena M, Nicquevert B, Mainaud Durand H, et al. Application of probabilistic modelling for the uncertainty evaluation of alignment measurements of large accelerators magnets assemblies. Meas Sci Technol 2018;29(5)https://iopscience.iop.org/article/10.1088/1361-6501/aaaca0.
[16] BIPM JCGM. 101 : evaluation of measurement data - Supplement 1 to the “ Guide to the expression of uncertainty in measurement ” - propagation of distributions using a Monte Carlo method. 2008. Paris.
[17] BIPM. International system of units (SI).vol. 339. 2006. doi:10.1007/BF00594162.
[18] JCGM. JCGM 200. International vocabulary of metrology - basic and general concepts and associated terms (VIM) 3rd edition Vocabulaire international de métrologie – concepts fondamentaux et généraux et termes associés (VIM) 3 e édition. 2012.
[19] Bryan JB, Doiron T. Temperature fundamentals. Coord. Meas. Mach. Syst. second ed. CRC Press; 2011. p. 273–303. https://doi.org/10.1201/b11022-11.
[20] California L, Brewer James Bryan Eldon R, McClure JW, Pearson WB, Bryan J, Pearson J, Brewer W, McClure E. Thermal effects in dimensional metrology vol. 87. 1965.
[21] ISO/TR. Geometrical product specifications (GPS) - systematic errors and contributions to measurement uncertainty of length measurement due to thermal influences. 2003. 16015.
[22] Weck M, McKeown P, Bonse R, Herbst U. Reduction and compensation of thermal errors in machine tools. CIRP Ann - Manuf Technol 1995. https://doi.org/10.1016/

S0007-8506(07)60506-X.
[23] Ramesh R, Mannan M, Poo A. Error compensation in machine tools - a review. Int J Mach Tool Manuf 2000;40:1257–84. https://doi.org/10.1016/S0890-6955(00)00010-9.
[24] Li JW, Zhang WJ, Yang GS, Tu XBC SD. Thermal-error modelling for complex physical systems: the-state-of-arts review. Int J Adv Manuf Technol 2008:168.
[25] Bryan JB. International status of thermal error research. Mech Eng CIRP 1967:25–50.
[26] Fransen S, Doyle D, Catanzaro B. Opto-mechanical modelling of the Herschel space telescope at ESA/ESTEC. Integr. Model. Complex Optomech. Syst. Vol. 8336. Int. Soc. Opt. Photonics 2011. https://doi.org/10.1117/12.915669.
[27] Ross-Pinnock D, Yang B, Maropoulos PG. Integration of thermal and dimensional measurement – a hybrid computational and physical measurement method. 38th MATADOR Conf.; 2015.
[28] Ross-Pinnock D, Bingru Yang Glen Mullineux B. Point-based models for compensation of thermal effects in dimensional metrology. Tools Methods Compet Eng 2016:117–28.
[29] Fong JT, Filliben JJ, DeWit R, Fields RJ, Bernstein B, Marcal PV. Uncertainty in finite element modelling and failure analysis: a metrology-based approach. J Press Vessel Technol ASME 2006;128:140–7. https://doi.org/10.1115/1.2150843.
[30] University of Bath UK (Lead RO, Aerotech Design Consultants (Collaboration), National Physical Laboratory NPL, United Kingdom (Collaboration PP, Renishaw Plc, United Kingdom (Collaboration PP, Airbus Group (Collaboration), Rolls Royce Group Plc (Collaboration), et al. The Light Controlled Factory Research project n.d. https://gtr.ukri.org/projects?ref=EP%2FK018124%2F1 (accessed November 3, 2018).
[31] Thery P, Raucoules F. Heat flux comparator. US 6994468 B2, 2006.
[32] 10K 3A1 series 1 thermistor specs n.d.
[33] Key Electronics Digi. DC95 - amphenol advanced sensors - thermistors NTC (negative temperature coefficient). Online Catalog | DigiKey Electronics; 2017https://www.digikey.com/catalog/en/partgroup/dc95/23406, Accessed date: 9 September 2017.
[34] K3 ATC. Chiller - applied thermal control. 2017http://app-therm.com/product/k3/, Accessed date: 16 August 2017.
[35] Wolf Z. A vibrating wire system for quadrupole fiducialization. LCLS Tech Notes 2005;1–23.
[36] Arpaia P, Caiazza D, Petrone C, Russenschuck S. Performance of the stretched and vibrating wire techniques and correction of background fields in locating quadrupole magnetic axes. Prague: XXI IMEKO world Congr. “measurement Res. Ind.; 2015.
[37] Temnykh A. Application of the vibrating wire technique for solenoid magnetic centre finding. 14th Int. Magn. Meas. Work. Cern. CERN; 2005.
[38] JCGM. Evaluation of measurement data - Guide to uncertainty in measurement. 2008.
[39] Borror CM, Montgomery DC, Myers RH. Evaluation of statistical designs for experiments involving noise variables. J Qual Technol 2002;34:54–70.
[40] Iman RL, Conover WJ. Small sample sensitivity analysis techniques for computer models.with an application to risk assessment. Commun Stat Theor Methods 1980;9:1749–842. https://doi.org/10.1080/03610928008827996.
[41] Florian A. An efficient sampling scheme: updated Latin Hypercube Sampling. Probabilist Eng Mech 1992;7:123–30. https://doi.org/10.1016/0266-8920(92)90015-A.
[42] Most T, Dynardo GmbH. Variance-based sensitivity analysis in the presence of correlated input variables 2010.
[43] Microconsult Engineering GmbH, Mai H. ANSYS & OptiSLang on an HPC-cluster. 2010.
[44] Phillips SD, Eberhardt KR, Parry B. Guidelines for expressing the uncertainty of measurement results containing uncorrected bias. J Res Natl Inst Stand Technol 1997;102:577. https://doi.org/10.6028/jres.102.039.
[45] Will J. OptiSLang inside ANSYS workbench. 2012.
[46] Fong J, Filliben J, Heckert A. Design of experiments approach to verification and uncertainty estimation of simulations based on Finite Elements Modeling. Pittsburgh, PA: Am. Soc. Eng. Educ.; 2008.
[47] Manteufel R. Evaluating the convergence of Latin hypercube sampling. 41st struct struct dyn mater conf exhib am inst aeronaut astronaut. 2000.
[48] Most T, Will J. Meta-model of Optimal Prognosis - an automatic approach for variable reduction and optimal meta-model selection. Proc. Weimarer Optimierungs-und Stochastiktage 2008;5:20–1.
[49] ISO/TS, ISO. ISO. 15530-4 Geometrical product specifications (GPS) - coordinate measuring machines (CMM): technique for determining the uncertainty of measurement - Part 4: evaluating task-specific measurement uncertainty using simulation. 2008.
[50] Leitz HexagonAB. PMM-C manufacturer website and descriptions. 2017 Last accessed on 09.2016 http://hexagonmi.com/products/coordinate-measuring-machines/bridge-cmms/leitz-pmmc.
[51] Carl Zeiss AG. ZEISS PRISMO CMM - manufacturer's website. 2017 (accessed June 20, 2017). https://www.zeiss.com/metrology/products/systems/bridge-type-cmms/prismo-navigator.html.
[52] Morishima T, Van Ostayen R, Van Eijk J, Schmidt RHM. Thermal displacement error compensation in temperature domain. Precis Eng 2015. https://doi.org/10.1016/j.precisioneng.2015.03.012.
[53] Schwenke H, Knapp W, Haitjema H, Weckenmann A, Schmitt R, Delbressine F. Geometric error measurement and compensation of machines-An update. CIRP Ann - Manuf Technol 2008;57:660–75. https://doi.org/10.1016/j.cirp.2008.09.008.
[54] Ni J, Wu SM. Dynamic modelling for machine tool thermal error compensation. Trans Soc Mech Eng J Manuf Sci Eng 2003;125(2):245–54.
[55] Friedman JH. On bias, variance, 0/1—loss, and the curse-of-dimensionality. Data Min Knowl Discov 1997;1:55–77. https://doi.org/10.1023/A:1009778005914.
[56] Yu L, Lai KK, Wang S, Huang W. A bias-variance-complexity trade-off Framework for complex system modeling. Berlin, Heidelberg: Springer; 2006. p. 518–27. https://doi.org/10.1007/11751540_55.
[57] Hero AO, Fessler JA, Usman M. Exploring estimator bias-variance tradeoffs using the uniform CR bound. IEEE Trans Signal Process 1996;44:2026–41. https://doi.org/10.1109/78.533723.
[58] Mainaud Durand H, Artoos K, Buzio M, Caiazza D, Catalan Lasheras N, Cherif A, et al. Main achievements of the PACMAN project for the alignment at micrometric scale of accelerator components. IPAC; 2017 2017.
[59] Schluse M, Rossmann J. From simulation to experimentable digital twins: simulation-based development and operation of complex technical systems. IEEE int symp syst eng 2016 2016. p. 1–6. https://doi.org/10.1109/SysEng.2016.7753162.
[60] Umetani N, Bickel B. Learning three-dimensional flow for interactive aerodynamic design. ACM Trans Graph 2018;37:1–10. https://doi.org/10.1145/3197517.3201325.
[61] Baqué P, Remelli E, Fleuret F, Fua P. Geodesic convolutional shape optimization. 2018. ArXiv Prepr ArXiv180204016.
[62] CERN. PACMAN innovative doctoral program. 2017https://pacman.web.cern.ch/, Accessed date: 31 July 2017.